Supplementary Information

Direct Observation of Anisotropy-Driven Formation of Amyloid Spherulites in Real-time by Super-resolution Microscopy

*Min Zhang, Henrik D. Pinholt, Xin Zhou, Søren S.-R. Bohr, Luca Banetta, Alessio Zaccone, Vito Foderà * and Nikos S. Hatzakis**

Methods

Human insulin (HI) labeling and spherulite preparation**.**
Alexa Fluor 647 NHS Ester (ThermoFisher Scientific) was dissolved in anhydrous-DMSO to a concentration of 2 mg/mL. 5 µL of the dye solution was added to 1 mL 5 mg/mL HI (91077C, Sigma-Aldrich, 95%) monomer solution, mixed gently and thoroughly. The mixed solution was allowed to react for ~2 hours at room temperature to complete the conjugation. After that the labeled protein was purified from the excess of free dye by a PD SpinTrap G-25 column (GE Healthcare), divided into aliquots and stored at -80 ^{o}C.

HI spherulites were formed in 0.5 M NaCl, 20% acetic acid (VWR Chemicals, 98%) solution with pH around 1.7. The ratio of labeled to unlabelled HI monomer was about 1 to 60000 (dSTORM) or 1 to 10000 (RE-PLOM), with the final concentration of HI was 5 mg/mL. The solution was filtered through 0.22 µm filters (LABSOLUTE) and then incubated in a block heater.

Atto 655-labeled liposome preparation for 3D dSTORM calibration.
Atto 655-labeled liposomes with 2% negative charge which were used for the 3D dSTORM calibration were prepared as previously published method [1]. In detail, a ratio of 97/2/0.5/0.5 for 1,2-Dioleoyl-sn-Glycero-3-Phosphocholine (DOPC), 1,2-dioleoyl-sn-glycero-3-phospho-L-serine (sodium salt) (DOPS), 1,2-distearoyl-snglycero-3-phosphoethanolamine-N-[biotinyl(polyethylene glycol)-2000] (ammonium salt) DSPE-PEG_{2000}-biotin and Atto655-PE were added to a glass vial. The solvent chloroform was removed completely by nitrogen flow for about 10 minutes followed by vacuum for several hours. The lipid film was rehydrated in MES buffer (pH 5.6) to final total lipid concentration 0.5 mg/mL, vortexed for 30 seconds and incubated for 30 minutes. The sample was extruded 11 times through a polycarbonate membrane filter with a pore size 50 nm. Then the liposome suspension was exposed to 10 cycle of flash-freezing and thawing so as to ensure an unilamellar membrane structure. The liposomes were aliquoted and stored at -20 ^{o}C.

Turbidity / Thioflavin T (ThT) fluorescence kinetics.

For in situ absorbance or ThT fluorescence, experiments were carried out using a plate reader system (BMG LABTECH, CLARIOstar) with 96-microwell polystyrene plates (Nalge Nunc, ThermoFisher Scientific). Each well contained 200 µL solution. The plates were covered with a self-adhesive sealing film (nerbe plus, for absorbance) or a clear polyolefin film with sealing tape (Thermo Fisher Scientific, for ThT fluorescence) to avoid evaporation of the samples and incubated at the desired temperatures without mechanical shaking. For absorbance, the excitation wavelength was 480 nm; and for ThT fluorescence, the solution contained 20 µM ThT and the emission intensity at 486 nm was recorded upon excitation at 450 nm. The signal was detected every 309 s.

REal-time kinetic via Photobleaching LOcalisation Microscopy (REPLOM).

Quantification of growth kinetics by Euclidean Minimum Spanning tree

The method for identification of candidates for fluorophores docking on a growing aggregate was inspired by recent published work [2] and done in the following way:
First, using all detected RE-PLOM spots from the movie, an approximate Euclidean Minimum Spanning tree was constructed using only the 30 nearest neighbors as candidates for edges. Regions of aggregate candidates were cut from each other by removing all edges with lengths more than the 95th percentile. This is an effective way of separating high-density regions from low-density regions. The computation was done using the function HierarchicalClustering from the astroML python package. Since we were interested mostly in the large insulin aggregates where the internal structure was visible, it was decided that all clusters obtained in this manner with less than 100 detected fluorophores were excluded from the subsequent analysis.

The time-dependency of the aggregate growth was found by a similar approach. At each frame, for a cluster, a refined grouping was done by cutting an approximate Euclidean Minimum Spanning tree made using 10 neighbors with a distance cutoff of 400nm which was found to be optimal for removal of most spots outside the aggregate while still not cutting up the main group. The points from the largest subgroup resulting from this analysis were defined to be the aggregate for that frame.

The area of the aggregate was estimated using a gaussian mixture model with a component for every 5 points in the aggregate, but not less than 25 components [2] . We defined the area of the aggregate as the region lying above the average probability density in this fit. The growth profile resulting from our approach had a few artifacts like jumps and fluctuations due to mixture model fitting and aggregate segmentation, but we found that the resulting growth curve in most cases had an identifiable trend, and the results were quite consistent across parameter choices.

From the estimated area of the aggregate in each frame, a growth curve could be plotted. The radial growth rate of such aggregates has previously been found to be either reaction-limited or diffusion-limited, leading to linear increase in time or increase as $\propto \sqrt{t}$ respectively[3-6]. If we assume that the estimated area of the aggregated is directly related to the radius as $A \propto R^2$ the two growth types lead to the following models

$$\frac{\mathrm{d}A(t)}{\mathrm{d}t} = r_1 ,$$

$$\frac{\mathrm{d}A(t)}{\mathrm{d}t} = \frac{1}{2} r_1 t .$$

Where the first model is diffusion limited and the second is reaction limited. We found that many of the structures where initially consistent with reaction limited diffusion and then shifted to either diffusion or reaction limited growth with a new rate. To allow for this shift, we let the growth be diffusion limited up to a switch-point t_0 after which the growth rate changes. We formulate one such model which ends reaction limited and one which remains diffusion limited

$$\frac{\mathrm{d}A(t)}{\mathrm{d}t} = \begin{cases} r_1, & t_0 > t \\ r_2 , & t_0 \leq t \end{cases} ,$$

$$\frac{\mathrm{d}A(t)}{\mathrm{d}t} = \begin{cases} r_1 , & t_0 > t \\ \frac{1}{2} r_2 \, t, & t_0 \leq t \end{cases} .$$

Finally, without continuous flow of constituent monomer, the growth inevitably saturates at a plateau[7]. For both models, we therefore introduce a switch time t_1 after which the growth slowly saturates sigmoidally over a time interval 5τ

$$\frac{\mathrm{d}A_{\mathrm{lin}}(t)}{\mathrm{d}t} = \begin{cases} r_1 , & t_0 > t \\ r_2 , & t_0 \leq t < t_1 \\ r_2 \dfrac{1}{1 + e^{\frac{5(t-\tau-t_1)}{\tau}}} , & t_1 \leq t \end{cases} ,$$

$$\frac{\mathrm{d}A_{\mathrm{par}}(t)}{\mathrm{d}t} = \begin{cases} r_1 , & t_0 > t \\ \frac{1}{2} r_2 t , & t_0 \leq t < t_1 \\ \frac{1}{2} r_2 \dfrac{t}{1 + e^{\frac{5(t-\tau-t_1)}{\tau}}} , & t_1 \leq t \end{cases} .$$

Where we introduced the names A_{lin} and A_{par} referring to the linear-like and parabolic-like shape of the two resulting growth curves. We found the anisotropic spherulites to fit best with A_{lin} and the isotropic spherulites fit best with A_{par}.

When fitting an experimentally observed aggregate growth curve $\{A_i, t_i\},\ i \in (0, N-1)$ the equations where numerically integrated from an initial timepoint (A_0, t_0) to the final timepoint (A_{N-1}, t_{N-1}). For each growth curve, the parameters $(r_1, r_2, t_0, t_1, \tau)$ were estimated with a chi2 fit. Each fit was run twice, the first fit was unweighted and were used to estimate the error bars using the standard deviation of the residuals. The second fit used the residuals in a weighted chi2 fit to obtain the final fit parameters for the growth curve.

Supplementary figures

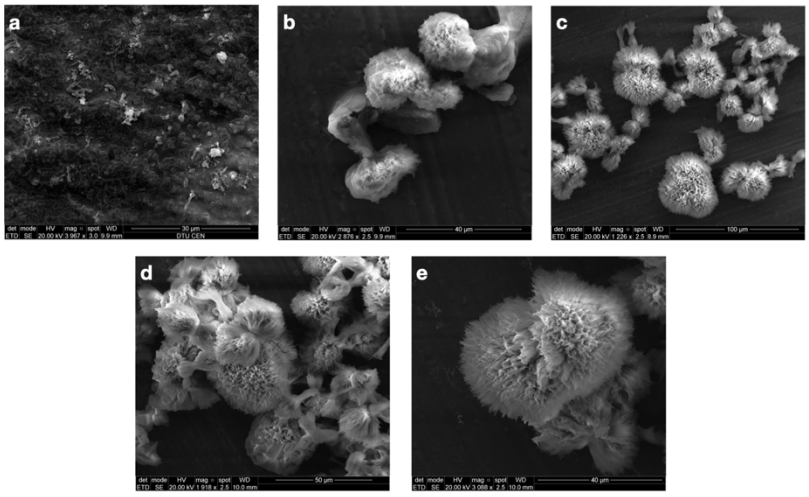

Supplementary Figure 1. SEM image of spherulites grew at 60 °C. (a) with incubation time of 1 hour, (b) with incubation time of 2 hours, (c) with incubation time of 4 hours and (d-e) with incubation time of 24 hours. (e) a fully-grown insulin spherulite. Scale bars are (a) 30 um, (b) 40 um, (c) 100 um, (d) 50 um and (e) 40 um respectively.

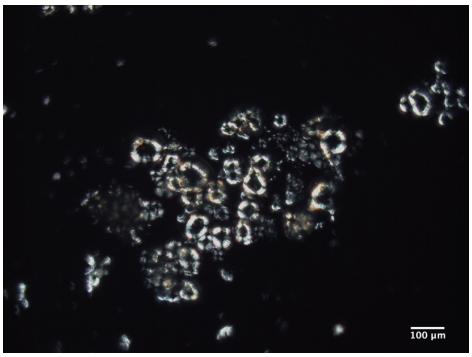

Supplementary Figure 2. Spherulites images obtained by cross polarised microscopy Zeiss Axioplan Optical Microscope, Carl Zeiss. The characteristic Maltese cross shows spherulite formation[8]. Scale bar is 100 um.

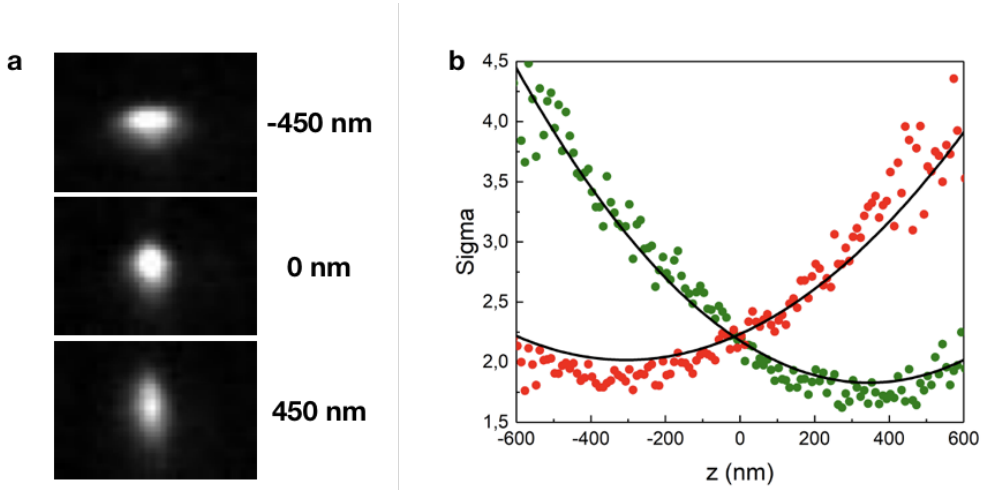

Supplementary Figure 3. (a) Single localisation imaging of Atto-655 labeled liposomes extruded at 50nm and tethered on poly-L-Lysine passivated surfaces. Calibration curve of PSF widths as a function of z. Z step length was 10 nm. The calibration curve was calculated by ThunderSTORM.

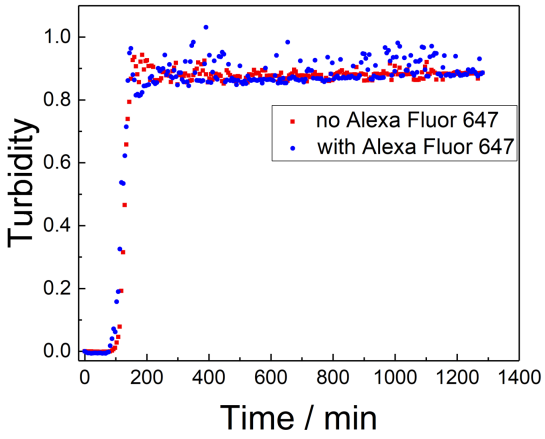

Supplementary Figure 4. Turbidity kinetics of human insulin at 60deg with and without Alexa 647. Each curve is the average on four replicates. The consistent of turbidities confirms that labeling doesn't interfere the aggregation process.

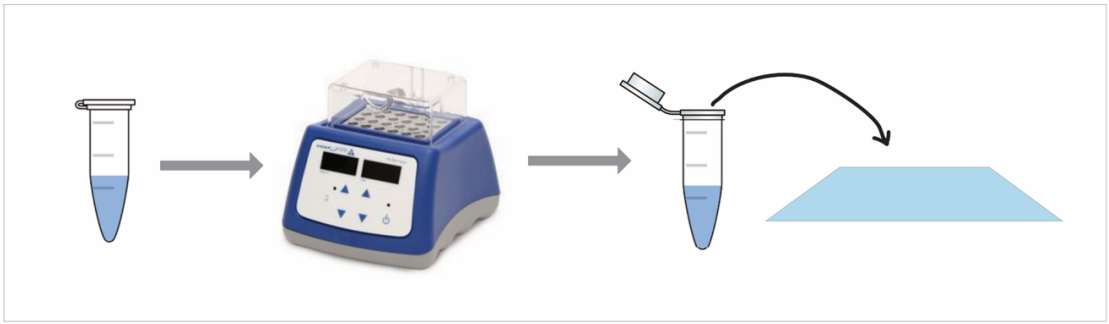

Supplementary Figure 5. All the samples were pre-incubated in a block heater in the designated temperature to skip the lag-phase. Preincubated samples were then put on a microscope slide to monitor spherulite growth on the microscope.

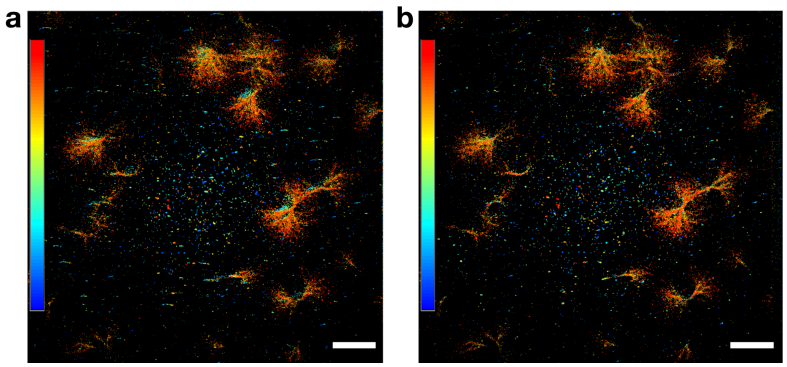

Supplementary Figure 6. RE-PLOM image of HI spherulites grown at 45 ℃ (a) prior to and (b) after drift correction. Scale bars: 10 um. The pseudocolor represents time and ranges from 0 s (blue) to 9500 s (red).

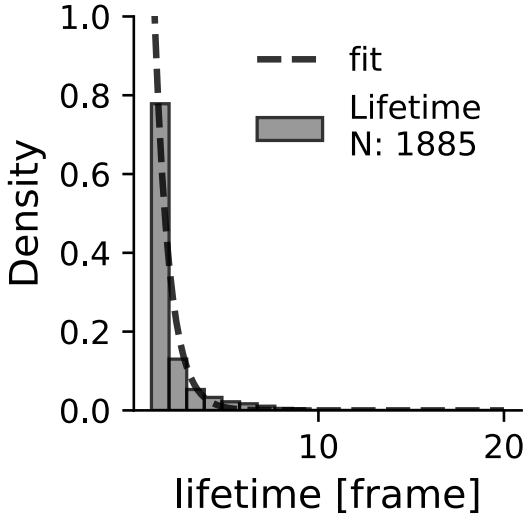

Supplementary Figure 7. Quantification of bleaching time of Alexa 647 in RE-PLOM conditions. In the experimental condition used (absence of imaging buffer and high laser power) Alexa 647 chromophores are rapidly photobleached. Lifetime is 0.7845 ± 0.0017 frames

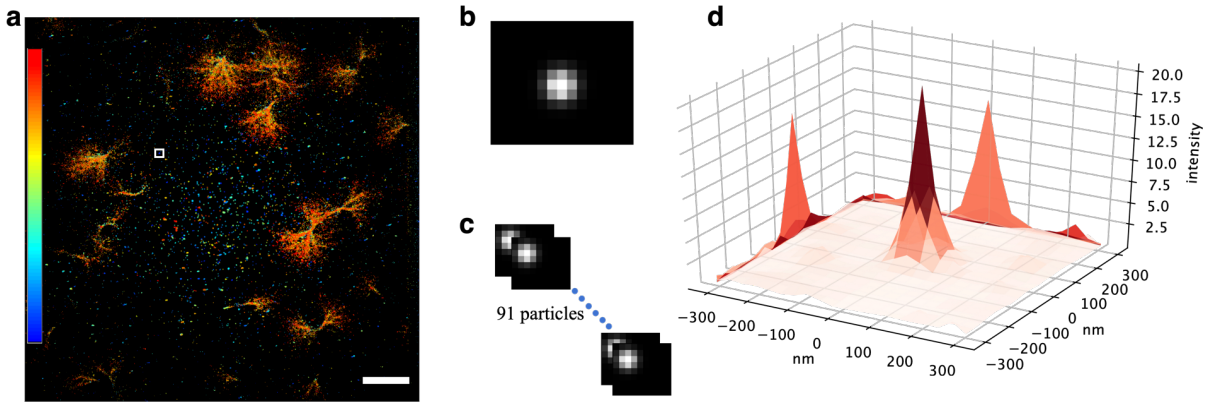

Supplementary Figure 8. Quantification of RE-PLOM resolution. (a) RE-PLOM image of HI spherulites grew at 45 ℃. Scale bar: 10 um. (b) Higher-magnification view of the boxed region in (a), which contains a single spot. (c) 91 particles were selected for resolution calculation. (d) Resulting 2D histograms were generated by aligning the 91 particles to the same center. Two-dimensional gaussian fitting to the presented histogram allowed extraction of FWHM for resolution determination. FWHM x: 68.1 nm, FWHM y: 66.2 nm.

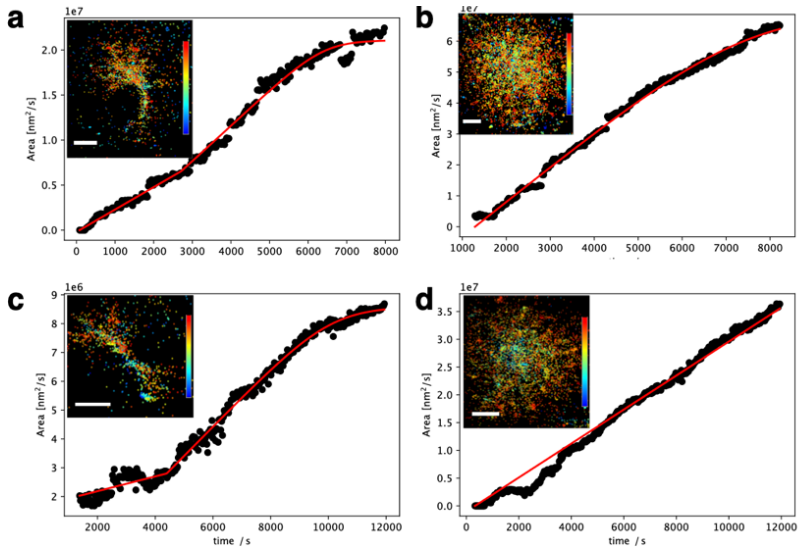

Supplementary Figure 9. Representative anisotropic (a,c) and isotropic (b,d) HI spherulites obtained by REPLOM and their corresponding growth curves. The incubation temperatures were: (a&b) 37 degrees, and (c&d) 32 degrees. Scale bars: 2 um. In The pseudocolor bar represents time and spans from 0s to 8000s in (a and b) and from 0 s to 12000 s in (c and d).

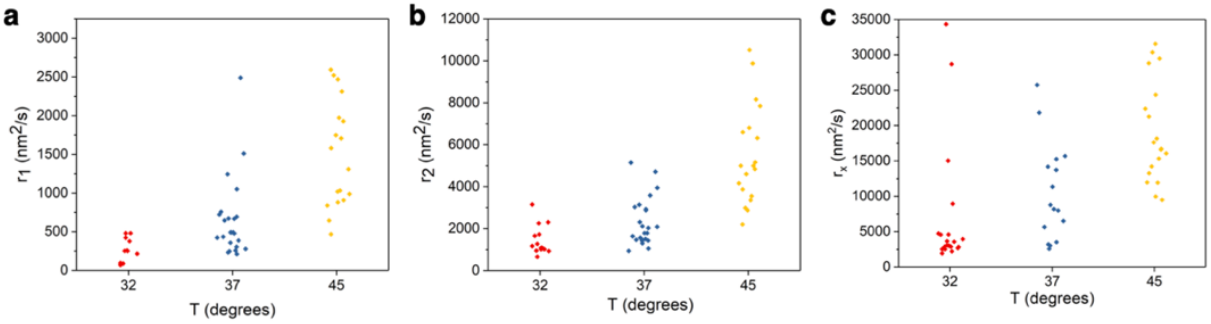

Supplementary Figure 10. Growth rate distribution for all tested temperatures (32, 37 and 45 degrees) for all spherulite growth morphologies. a) for r_1 of anisotropic growth b) for r_2 of anisotropic growth c) r_x for isotropic growth. Data extracted from Arrhenius plots in figure 4.

Supplementary Table 1. Quantification of the diameters of the central fibrils of the intermediates in Fig 2c.

Intermediates in Figure 2c		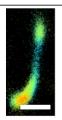	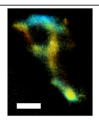	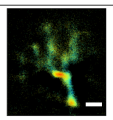	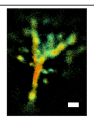	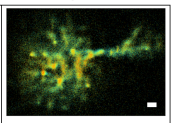
Diameter of the central fibrils (nm)	~300	~400	~450	~450	~600	~700

References

1 Thomsen, R. P. *et al.* A large size-selective DNA nanopore with sensing applications. *Nat. Commun.* **10**, 5655, doi:10.1038/s41467-019-13284-1 (2019).

2 Cowan, N. B. & Ivezić, Ž. The Environment of Galaxies at Low Redshift. *The Astrophysical Journal* **674**, L13-L16, doi:10.1086/528986 (2008).

3 Goldenfeld, N. Theory of spherulitic crystallization. *Journal of Crystal Growth* **84**, 601-608, doi:https://doi.org/10.1016/0022-0248(87)90051-0 (1987).

4 Domike, K. R. & Donald, A. M. Thermal Dependence of Thermally Induced Protein Spherulite Formation and Growth: Kinetics of β-lactoglobulin and Insulin. *Biomacromolecules* **8**, 3930-3937, doi:10.1021/bm7009224 (2007).

5 Majumder, S., Busch, H., Poudel, P., Mecking, S. & Reiter, G. Growth Kinetics of Stacks of Lamellar Polymer Crystals. *Macromolecules* **51**, 8738-8745, doi:10.1021/acs.macromol.8b01765 (2018).

6 Tanaka, H. & Nishi, T. New Types of Phase Separation Behavior during the Crystallization Process in Polymer Blends with Phase Diagram. *Physical Review Letters* **55**, 1102-1105, doi:10.1103/PhysRevLett.55.1102 (1985).

7 Domike, K. R. & Donald, A. M. Kinetics of spherulite formation and growth: Salt and protein concentration dependence on proteins β-lactoglobulin and insulin. *International Journal of Biological Macromolecules* **44**, 301-310, doi:https://doi.org/10.1016/j.ijbiomac.2008.12.014 (2009).

8 Krebs, M. R. H. *et al.* The formation of spherulites by amyloid fibrils of bovine insulin. *Proceedings of the National Academy of Sciences of the United States of America* **101**, 14420-14424, doi:10.1073/pnas.0405933101 (2004).